OPEN ACCESS
IOP Publishing
Superconductor Science and Technology
Supercond. Sci. Technol. 29 (2016) 075005 (16pp)
doi:10.1088/0953-2048/29/7/075005

Soldered joints—an essential component of demountable high temperature superconducting fusion magnets

Yeekin Tsui[1], Elizabeth Surrey[2] and Damian Hampshire[1]

[1] Department of Physics, Superconductivity Group, University of Durham, South Road, Durham, DH1 3LE, UK
[2] EURATOM/CCFE Fusion Association, Culham Science Centre, Abingdon, Oxon, OX14 3DB, UK

E-mail: d.p.hampshire@durham.ac.uk

Received 19 October 2015, revised 21 January 2016
Accepted for publication 7 March 2016
Published 23 May 2016

The figures in this version of the paper are editable. All data are accessible

In addition, we have also produced an Excel file which has all the data in the figures available on request from Prof. Hampshire

Soldered Joints – An Essential Component of Demountable High Temperature Superconducting Fusion Magnets

Yeekin Tsui[1], Elizabeth Surrey[2] and Damian Hampshire[1]

[1]Department of Physics, Superconductivity Group, University of Durham, South Road, Durham, DH1 3LE, UK.
[2]EURATOM/CCFE Fusion Association, Culham Science Centre, Abingdon, Oxon, OX14 3DB, UK.

Abstract

Demountable superconducting magnet coils would offer significant benefits to commercial nuclear fusion power plants. Whether large pressed joints or large soldered joints provide the solution for demountable fusion magnets, a critical component or building block for both will be the many, smaller-scale joints that enable the supercurrent to leave the superconducting layer, cross the superconducting tape and pass into the solder that lies between the tape and the conductor that eventually provides one of the demountable surfaces. This paper considers the electrical and thermal properties of this essential component part of demountable high temperature superconducting (HTS) joints by considering the fabrication and properties of jointed high temperature superconductors consisting of a thin layer of solder ($In_{52}Sn_{48}$ or $Pb_{38}Sn_{62}$) sandwiched between two Rare-Earth-$Ba_2Cu_3O_7$ (REBCO) 2G HTS coated conductors. The HTS joints are analysed using numerical modelling, critical current and resistivity measurements on the joints from 300 to 4.2 K in applied magnetic fields up to 12 T, as well as scanning electron microscopy studies. Our results show that the copper/silver layers significantly reduce the heating in the joints to less than a few hundred mK. When the REBCO alone is superconducting, the joint resistivity (R_J) predominantly has two sources, the solder layer and an interfacial resistivity at the REBCO/silver interface (~25 n$\Omega\cdot$cm^2) in the as-supplied coated conductors which together have a very weak magnetoresistance in fields up to 12 T. We achieved excellent reproducibility in the R_J of the $In_{52}Sn_{48}$ soldered joints of better than 10 % at temperatures below T_c of the REBCO layer which can be compared to variations of more than two orders of magnitude in the literature. We also show that demountable joints in fusion energy magnets are viable and need only add a few percent to the total cryogenic cost for a fusion tokamak.

1. Introduction

Recent improvements [1] in the current density of coated conductors (CCs) with high temperature superconductors (HTS) using self-assembling pinning sites have driven it up to values as high as a few percent of its theoretical limit in high magnetic fields. Together with the very high upper critical fields and critical temperature of these materials, this has encouraged development of high-field HTS magnets and brightened the prospects of higher field fusion machines [2]. Since there are still no ductile high-field superconductors that can produce magnet fields above about ~ 10 T, toroidal field (TF) magnets in future tokamaks will still have to include one of the many brittle high-field superconductors, and the life-cycle of a commercial fusion machine must include economic options for replacing these coils. In this paper we investigate whether the properties of HTS materials can help mitigate the costs of replacing TF coils, by enabling demountable joints [3-6]. Demountable joints will: eliminate the single point failure of a monolithic TF coil structure; enable the modular construction of very large complex superconducting magnets; improve reactor maintenance by improving access; increase the availability of a fusion reactor; enable simplified materials component testing; and open the possibility of novel topologies for fusion reactors which are not otherwise practical. We have studied small simple soldered joints consisting of a thin layer of solder sandwiched between two Rare-Earth-$Ba_2Cu_3O_7$ (REBCO) 2G HTS coated conductors. Although these hand-made joints will probably not provide the solution for large-scale commercial joints in a tokamak by themselves, understanding this basic building block of joints is essential for evaluating and optimizing larger mechanically pressed or soldered joints because transfer of current out of an HTS layer and across solder into a normal metal is a process that is unavoidable in most practical large tokamak-relevant joint designs. Our results can also provide useful information for the design of general high-field magnets which involve joining HTS coated conductors [7, 8]. We present numerical analysis, resistivity measurements, critical current measurements from 300 to 4 K and in applied magnetic fields up to 12 T as well as scanning electron microscopy (SEM) images of the HTS soldered joints fabricated using $In_{52}Sn_{48}$ and $Pb_{38}Sn_{62}$ solders. The contents of this paper are arranged as follows: background information is included in section 2; the description of the fabrication, structure and components of the joints is in section 3; section 4 includes the finite element analysis; section 5 describes the cryogenic measurements and results; the last two sections use our results and understanding of joints to calculate the expected

cryogenic cost of demountable joints in fusion applications, summarizes the important conclusions and briefly discusses our on-going and future work.

2. Background

The value of demountable joints has long been appreciated [9-12]. Designs of magnets with demountable joints for tokamak [13] and heliotron [14] reactors were proposed in 1980s. However, the heat generated by these joints in low temperature superconductor (LTS) were considered so high as to undermine the stability of the magnets [15] and as a result, the demountable option was not included in fusion reactor designs such as the ITER tokamak [16]. The ITER TF systems consist of 18 TF coils, each of which comprise of seven double pancakes sub-coils connected by 6 praying-hands joints and 2 shaking hands joints connected to the feeder bus bars. These joints carry 68 kA and have resistances of ~ 1 nΩ to ensure the static heat dissipation is within the 5W design limits [17, 18], but use a wind and react type process so are permanent [19, 20]. Techniques for making permanent joints with low-temperature superconductors (LTS) are well established [21] and include so-called persistent joints with extremely low joint resistance ($\leq 10^{-13}\,\Omega$) for MRI applications [22]. Recently, there has also been success in fabricating persistent joints using HTS [23]. However, because it is very time-consuming and demanding to fabricate hand-made persistent joints at elevated temperatures, they are not useful for commercial fusion applications. Although the optimum design of the joints for fusion energy is currently an open question, any practical solutions will avoid making several million demountable tape-to-tape or strand-to-strand joints sequentially.

There are essentially two types of resistive joints reported in the HTS literature, the lap (or bridge) joint which maximises contact area to achieve low resistance and the butt (or edge) joint where the priority is to minimise the separation of the superconductors. HTS lap joints are most successful to date because the demountable interfaces are metallic whereas butt joints are susceptible to mechanical damage [3, 7, 24, 25]. There are many groups working on connecting multiple strands or tapes using soldered joints. Hartwig *et al.* have proposed a demountable toroidal field (TF) coil design for a small tokamak [3]. Each joint in the TF coil is made out of a stack REBCO coated conductors (CCs) which are joined mechanically. Kawai *et al.* have proposed a demountable helical coils (HC) design for a force free helical reactor at NIFS [24-26] and have produced total joint resistances in the nΩ range. In this design, two conductors are

joined together mechanically by the ends or edges that may also be soldered using a bridging unit. A cooling system that uses bronze sintered porous media with sub-cooled liquid nitrogen was proposed to remove the heat generated at these joints under operating conditions to make the demountable helical reactor design more feasible [15]. HTS power transmission cable projects [27-29] may also offer fusion relevant solutions for joints [28, 29]. For example the 275 kV-3kA, 30 m HTS cable system from Yagi et al. [28] demonstrates that soldered joints remain robust in a demanding AC environment. There is also a creative cable termination design reported by Takayasu et al. that has been developed for an HTS cable made of stacked REBCO and BiSCCO tapes [27]. The asymmetric electric property of REBCO tapes is overcome by soldering REBCO tapes onto symmetric BiSCCO tapes.

Large TF coils are designed to carry very high currents of 10 kA – 100 kA to produce high magnetic fields without generating high voltages. In standard power engineering, conventional joints between cables carrying high currents are ubiquitous. Experiments using current pulses of ~ 250 kA include those at lightning test laboratories [30] and those on circuit breaker devices for use in the power generation and distribution industry [31]. Industrial areas that use continuous high currents up to 400 kA include electrolysis plants [32] and industrial furnaces [33]. Although there is not a 'standard' high current joint design, the vast majority of joints in the power engineering sector are straightforward, mechanically pressed, welded or bolted joints which offer design options for fusion energy applications.

There is also work on a smaller scale, looking at joining a few tapes and the detail of how the supercurrent leaves the HTS superconductor, crosses the normal metal layers and re-enters another HTS superconductor. This includes investigating how to design and fabricate such joints for use in HTS laboratory high-field magnets [7, 8]. In such work, HTS CCs are simply soldered directly together. Soldering has been widely used for joining second generation (2G) HTS CCs because of the simplicity of the fabrication technique, the reasonably low joint resistivity (R_J) achieved and the lack of additional structures needed to ensure mechanical joints remain intact under pressure. However, because of the multilayer structure of the 2G CCs, and the sensitivity of the brittle tapes to mechanical stress and elevated processing temperature, technical problems remain in soldering 2G CCs. The range of R_J values reported in the literature is large. The R_J of similar soldered joints with the same CCs can vary from ~ 4 to over 1000 nΩ·cm^2 at 77 K [7, 34-36]. Inconsistent results are also found in the magnetic field dependence of R_J. Some studies

claimed that there was no observable field dependence of R_J [7, 36]. Other studies demonstrated that R_J of the samples fabricated using the same kind of CCs changed significantly with an applied magnetic field [37]. If resistive demountable joints are to help enable commercial fusion, they must be robust and reproducible and their resistances must be low enough under all operating conditions (e.g. in-field) to avoid large cryogenic costs or quenching the superconductor. There are also only limited studies on the temperature dependence of R_J [37-39] which to date has meant there is no model for describing R_J accurately nor is there a reliable estimate of the joint resistivity expected under operating conditions for different applications. Small scale, soldered joints will be an integral component of any large fusion joint between superconductors and are the focus of this paper. We fabricate the small joints, and investigate their resistive and thermal properties. Our numerical results allow us to calculate the heating in these resistive soldered joints when they are subjected to an electric current. Our experimental results explain the inconsistent findings in R_J in the literature and allow us to propose a simple but accurate model for R_J.

3. Fabrication of the Joints and their component properties

3.1. *Joint fabrication*

All joints were fabricated using SuperPower Inc. IBAD-MOCVD 2G REBCO coated conductor tapes [40]. We note that these tapes are not optimized for fusion applications - silver can become strongly active under a neutron flux [41]. The specifications of the tapes are listed in Table 1 and a schematic diagram of its multilayer structure shown in Figure 1. The tapes are produced by SuperPower Inc. from wider tapes and sliced down to 4 mm wide strips. The length of the joints made were typically about 4 mm. SuperPower Inc. recommends soldering to them at or below 250 °C [42]. Table 2**,** provides properties from our survey and measurement of many low temperature solders. Two solders were selected and fabricated from elemental powders in-house: $Pb_{38}Sn_{62}$ because it has the lowest resistivity of the alloys at 77 K, it is the eutectic composition (from phase diagram studies [43]) with a melting point of 183 °C and has been widely used in

the literature to join REBCO CCs and $In_{52}Sn_{48}$ because of its lower melting point (118 °C), low resistivity and because thermal properties are rather well-known compared to other similar choices.

Each joint studied in this work was soldered in air using a temperature controlled soldering iron, preset to 250 °C for $Pb_{38}Sn_{62}$ solder or 190 °C for $In_{52}Sn_{48}$ solder, with the REBCO layers face to face. The solder was first prepared in the form of foil with thickness of about 50 μm and then placed between two pre-fluxed REBCO tapes. The tapes were held down on a flat surface that was covered in an insulating Kapton layer. Kapton tape was used to temporarily fix the tape to the layer and heat was then applied to the tapes to join them together. The joints are characterised by a joint resistivity (R_J) in $n\Omega \cdot cm^2$, which is an intensive property given by the product of the resistance and the area of the joint. Since all solders and joints were prepared in air, we expect some small oxide content in the solder increases their resistivity by a few percent.

3.2. *The Structure of the Joints*

A Hitachi Tabletop TM 1000 Scanning Electron Microscope was used to obtain all SEM images. Cross sectional SEM images of joints made using the two different solders are shown in Figure 2 ($In_{52}Sn_{48}$) and Figure 3 ($Pb_{38}Sn_{62}$). In addition to the solder layer, there is a thin continuous layer of intermetallic compound between the solder layer and the copper stabilizer which indicates good metallurgical bonding [44]. The typical thickness of the solder layer is ~ 22 μm for both solders which at 77 K contributes roughly 10 $n\Omega \cdot cm^2$ for $Pb_{38}Sn_{62}$ and 30 $n\Omega \cdot cm^2$ for $In_{52}Sn_{48}$ solder to the joint resistivity. Although thinner solder layers with lower joint resistivities can be achieved by applying large pressures during fabrication, we chose not to use that approach here in order to avoid damaging the brittle REBCO and to achieve better reproducibility of results [45, 46]. In the SEM image of the $Pb_{38}Sn_{62}$ joint there is a clear gap of ~ 7 μm in or close to the REBCO layer. We suggest this delamination may have occurred because of the higher soldering temperature used with $Pb_{38}Sn_{62}$ solder and helps explain the greater variability, we find in this work and found in the literature, for joints fabricated using $Pb_{38}Sn_{62}$ solder.

3.3. *The Superconducting solders $Pb_{38}Sn_{62}$ and $In_{52}Sn_{48}$*

The normal-state resistivity and superconducting properties in-field of both $Pb_{38}Sn_{62}$ and $In_{52}Sn_{48}$ solders used in the joints were measured at different temperatures and magnetic fields. In these measurements the solder served both as the sample and as the material for connecting the instrumentation leads. Figure 4 shows normal state properties below 300 K. $Pb_{38}Sn_{62}$ solder has a much lower resistivity than $In_{52}Sn_{48}$ solder at low temperatures. We also included data for the widely used non-eutectic commercial solder $Pb_{40}Sn_{60}$ for comparison. Figure 4 shows low temperature in-field data and the superconducting phase diagrams.

4. Finite element analysis of temperature and voltages in joints.

Numerical calculations of current flow through the joints and the resulting temperature profile were made using a commercial finite element analysis (FEA) package (FlexPDE^{TM}). During the fabrication of REBCO tapes, they are first cut (or slit) to the required width and then electroplated with copper. The multilayered structure of the joint that we have modelled is shown in Figure 6 and does not include copper on the sides of the tape. We have omitted this Cu because it often becomes partially detached from the tapes and by omitting it, our FEA calculations and conclusions are relevant not just for the narrow tapes investigated here, but also for the wider tapes that may be used in large scale fusion devices. The resistivity and thermal conductivity of different components of a joint used for the computations are listed in Table 3 and were obtained either from the literature or in-house measurements. The buffer stack has been ignored because it is very thin and we find experimentally that the two copper layers are electrically well-connected. In the FEA, we assume the joint is completely surrounded by liquid helium (4.2 K) or nitrogen (77 K), as is the case for our experiments below, with cryogen properties given in Table 4. By solving Laplace's equation:

$$\nabla^2 V = 0, \qquad 4.1$$

where V is the voltage, together with the boundary conditions necessary to inject and extract current, the electrical field throughout the system is calculated. From the electrical conductivity of the components of the joint, the current density flowing and the power density dissipated

throughout the joint are then obtained. From the definition of the thermal conductivity and the conservation of energy, in steady state one can derive:

$$\nabla^2 T + \frac{1}{\kappa_n \sigma_n} J^2 = 0, \qquad 4.2$$

where J, T, σ_n and κ_n are the current density, temperature, electrical and thermal conductivity of the solid components in the joint respectively. Solving Eqn. 4.2 then gives the temperature profile throughout the joint. Accurate knowledge of the heat flux across the boundaries of the joint into the cryogen is demanding, because both conduction and convection are important. If we simply assume the edges of the joint are at the temperature of the cryogen, we overestimate the heat transfer into the cryogen. Equally, assuming the cryogen is simply a solid with finite thermal conductivity underestimates the heat transfer into the cryogen by ignoring convection. In this paper we follow standard cryogenic engineering approximations for describing heat flux across a heated surface into a cryogen (cf Equations 4.3 – 4.10) [47]. We assume heat transfer is governed by Newton's law of cooling:

$$\frac{\dot{q}}{A} = -h(T_s - T_{Cryo}) \qquad 4.3$$

where $\dot{q}/A$ is the heat flux, h is the heat transfer coefficient, T_s is the temperature at the surface and T_{Cryo} is the temperature far from the heat sources (i.e. the boiling point of the cryogen). The heat transfer coefficient (h) is written in terms of the Nusselt number (N_u) where

$$h = N_u \frac{\kappa_{Cryo}}{L} \qquad 4.4$$

κ_{Cryo} is the thermal conductivity of the cryogen and L is a characteristic length of the geometry where for horizontal surfaces:

$$L = \frac{\text{Surface Area}}{\text{Perimeter}} \qquad 4.5$$

whereas for vertical surfaces, L is simply the height of the surface. The Nusselt number is written in terms of the Rayleigh number (R_a) that includes the role of buoyancy (or equivalently the orientation of the solid surface with respect to gravity) and viscosity. For conduction through the

upper surface of a heated plate (or the lower surface of a cooled plate) with low heat flux the Nusselt number is given by :

$$N_u = 0.54R_a^{1/4} \quad (10^4 \leq R_a \leq 10^7) \tag{4.6}$$

and for high heat flux

$$N_u = 0.15R_a^{1/3} \quad (10^7 \leq R_a \leq 10^{11}) \tag{4.7}$$

In this work we find $R_a \sim 10^6$ and so we use Eqn. 4.6. rather than Eqn. 4.7. For the lower surface of a heated plate, where buoyancy is less effective at contributing to heat transfer, one finds:

$$N_u = 0.27R_a^{1/4} \quad (10^5 \leq R_a \leq 10^{10}) \tag{4.8}$$

and for conduction through the heated side of a vertical plate:

$$N_u = \left\{ 0.68 + \frac{0.38R_a^{1/4}}{\left[1 + \left(\frac{0.492\alpha}{\nu}\right)^{9/16}\right]^{4/9}} \right\} \tag{4.9}$$

where the Rayleigh number is given by:

$$R_a = \frac{\text{Buoyancy Forces}}{\text{Viscous Drag}} = \frac{g\beta\left(T_S - T_{Cryo}\right)L^3}{\nu\alpha} \tag{4.10}$$

where $\alpha = \frac{\kappa_{Cryo}}{\rho c_p}$, g is the gravitational acceleration (9.8 m.s^{-2}), and β, ν, α, ρ and c_p are the thermal expansion, kinematic viscosity, thermal diffusivity, density and specific heat capacity of the cryogen respectively.

The FEA calculations were validated by comparison with analytic solutions for the electric field, current density and temperature profile in an infinite vertical cylinder of solder in cryogen carrying 100 A. The equivalent FEA solutions were obtained for an idealised joint which consists of a 20 micron vertical-cylinder of solder sandwiched between two slabs of thermally insulating, electrically conducting superconductor at the top and bottom also carrying 100 A, as

shown in Figure 7. The two-dimensional analytic solution for the temperature difference between the centre of the cylinder $\boldsymbol{T_{\mathbf{Centre}}}$ and the bulk of the cryogen ($\boldsymbol{T_{\mathbf{Cryo}}}$) is given by:

$$\Delta T = T_{\mathrm{Centre}} - T_{\mathrm{Cryo}} = \frac{J^2 {r_0}^2}{4\kappa_{\mathrm{n}}\sigma_{\mathrm{n}}}\left\{1 + \frac{2\kappa_{\mathrm{n}}}{h r_0}\right\} \qquad 4.11$$

where the term in curly brackets in Eqn. 4.11 tends to unity in the limit that the thermal conductivity of the cryogen is taken to be infinite or that the surface of the joint is at the temperature of the cryogen. Since h is a function of ΔT, this transcendental equation must be solved numerically using Eqns. 4.4 – 4.10. Using the materials properties data listed in Table 3 for 77 K, we found the agreement between the FEA calculations of ΔT and the analytic solutions is good, as shown in Table 5. The temperature profile predicted from equation 4.11 and the FEA results shown in Figure 7 are also in good agreement. The FEA visualization results also show that the electric field and the resistive current density are quite uniform within the solder and that if there are no voltage taps across the solder itself, there is a discontinuous change in voltage between taps on one superconducting slab from those on the other one, independent of whether they are in the joint region above the solder or not. We also modelled the multilayered soldered joint (cf Figure 6). FEA shows the current density flow is quite uniform between the superconducting layers through the solder/copper/silver layers (similar to the results in Figure 7) and that most of the heat leaves along the copper/silver layers which significantly reduces the temperature inside the joint. Figure 8 shows the temperature profile throughout the joint. The temperature is rather uniform in the solder and in those parts of the tapes attached to the solder. In the approximation that all the heat leaves the joint along the four copper layers, we can derive an analytic equation for the maximum temperature in the joint (ΔT):

$$\Delta T = T_{\mathrm{Multilayer}} - T_{\mathrm{Cryo}} = \dot{q}\sqrt{\frac{1}{\kappa_{\mathrm{Cu}} A_{Cu} d_{Cu} h(\Delta T)}}\,, \qquad 4.12$$

where $\dot{q}$ is power along each copper sheet, κ_{Cu} is the thermal conductivity of the copper, A_{Cu} is the cross sectional area of each sheet and d_{Cu} is the length, orthogonal to the direction of heat flow for the surface through which the heat passes into the cryogen. For the tapes considered here, $\Delta T = \dot{q}_{Total}/4\sqrt{\kappa_{\mathrm{Cu}} wt(w+2t)h}$ where w and t are the width (4 mm) and thickness of

each copper layer (20 μm) respectively. At 77 K where the copper layer conducts much more heat than the thin silver layer, there is reasonable agreement between Eqn. 4.12 and the FEA calculations as shown in Table 5.

5. Cryogenic Experiments and Results

5.1. *Variable temperature resistivity measurements*

Cryogenic resistivity measurements were performed either in a 9 T Quantum Design PPMS system or in a Janis cryocooler at temperatures from 300 to 3 K. For each resistivity data point, Ohm's law was measured using currents up to 100 mA with the voltage taps typically 10 mm apart. Figure 9 shows data for a joint with the voltage taps distributed along the upper surface. The voltage for all taps on either one of the REBCO CCs was the same, but shows a discontinuity across the soldered joint, confirming the FEA result that the resistive current is restricted within the joint. We have measured the voltages generated across many CC joints under various conditions. If the current leads are too close to the voltage taps (less than a few millimetres), the voltage taps pick up some of the current transfer voltage. The current transfer voltages are particularly pronounced if the current crosses the high resistivity Hastelloy substrate (see Table 3) and can lead to a misleading and much higher apparent joint resistivity (R_J). Therefore, in general we put all the electrical leads on the side of the tape closest to the superconducting layer.

Typical temperature dependencies for the R_J of joints fabricated using the two different solders at zero applied magnetic field are plotted in Figure 10. At temperatures above 90 K, the REBCO tape was not superconducting and large resistivities, associated with all the normal material components between the voltage taps, are found. As the REBCO becomes superconducting, R_J drops by a few orders of magnitude. Eventually, the REBCO layer is completely superconducting and the $R_J(T)$ measured is due from the resistive parts of the joint, which includes the solder layer, the silver and copper sandwiched above and below the solder, and any interfacial resistivities between different layers of the REBCO CCs. As shown in Figure 10 -12, we attribute the joint resistivity predominantly to just two sources: a contribution to the joint resistivity from the solder (R_{solder}) because of its bulk temperature dependent resistivity and an

interfacial resistivity (R_i) between the REBCO and the silver layers. The joint resistivity, R_J, is given by:

$$R_J = R_{\text{solder}} + R_i \,. \qquad 5.13$$

The contribution from the bulk resistivities of the copper and silver can be considered negligible. The Cu and Ag may dissolve to form a binary alloy layer. The resistivity of Cu/Ag alloys is typically 25 % higher than that of pure Ag [48]. Since the Ag layer in a single HTS tape is only 2 μm thick, this sets the upper limit to the contribution of any Cu/Ag alloy to the joint resistivity to be less than 1 nΩ·cm^2 which can also be ignored. Figure 11 and Figure 12 display the temperature dependence of R_J from 90 K down to the lowest temperature studied (~ 4 K) for five $In_{52}Sn_{48}$ joints and six $Pb_{38}Sn_{62}$ joints. The width and length of each joint measured are given in the captions. All the $In_{52}Sn_{48}$ joints in Figure 11 show very straightforward, almost text-book, behaviour following Equation 5.13 - the average fitted values of the thickness of the solder layers was 22 μm with a standard deviation of 2 μm which are consistent values from the SEM and the interfacial resistivity is temperature independent with values of 20 to 27 nΩ·cm^2 – similar to those reported in the literature and attributed to the REBCO/Ag interface [49, 50]. The average difference between 5.13 and the measured values of R_J is 2.3 % in the temperature range of 8 K to 80 K, demonstrating excellent agreement. We have added interfacial resistances into our FEA calculations. Preliminary results show that, consistent with Figure 8, the maximum temperature is determined by the total heat generated by the joint and the temperature profile remains reasonably constant in the joint region, broadly unaffected by how the resistance is distributed throughout the joint. The interfacial resistivity values found experimentally here can be compared with the much higher typical values for domain walls in ferromagnetic materials where $R_i \sim 10^{-7}$ Ω·cm^2 or domain walls in single crystal antiferromagnetic materials where $R_i \sim 10^{-5}$ Ω·cm^2 [51]. We note further reductions in joint resistivity have been achieved by reducing the thickness of the solder layer by applying high pressure during the fabrication process to reduce the solder layer thickness to just 1 to 2 μm [36]. Equally, we expect that the REBCO/Ag interfacial resistivity can also be substantially reduced by annealing REBCO/Ag in oxygen. A reduction in the resistivity of REBCO/Ag contacts to ~ 0.1 nΩ·cm^2 has been achieved by annealing for 1 hour at temperature above ~ 500 °C which diffuses some of the silver into the REBCO [52]. The data shown in Figure 12 for the $Pb_{38}Sn_{62}$ joints has larger variability than for

$In_{52}Sn_{48}$ – a result we associate with the higher temperature used in fabrication. In our first $Pb_{38}Sn_{62}$ joints, fabricated at temperatures higher than 270 °C (not otherwise reported here), R_J was always higher than 100 nΩ·cm^2 at 77 K. Although equation (5.13) fits $R_J(T)$ well for 2 of the 6 $Pb_{38}Sn_{62}$ joints (Joints 11 and 12) with reasonable values for solder layer thickness (23 and 25 μm) and for R_i (24 and 26 nΩ·cm^2 – similar to the $In_{52}Sn_{48}$ joints), the reproducibility of $Pb_{38}Sn_{62}$ joints was far worse than the $In_{52}Sn_{48}$ joints and non-physical values for the solder layer thickness (35 to 90 μm) needed to fit the joint resistivity data for the other 4 $Pb_{38}Sn_{62}$ joints. Nevertheless, because $Pb_{38}Sn_{62}$ solder has better wetting properties [53] and lower resistivity than $In_{52}Sn_{48}$ solder (see Figure 10) although the properties of the joints were unreliable, we found it produced the very lowest resistivity joints reported in this paper.

At temperatures just below the critical temperature of the superconducting solder, there is another sudden drop in $R_J(T)$. The $In_{52}Sn_{48}$ joints continue to obey Equation 5.13 below 6 K and $R_J(T)$ becomes just the interfacial resistivity (all joints except joint 5) as expected. However the $Pb_{38}Sn_{62}$ joints are more complex below 7 K. The resistivity of these joints continued to drop to very low values (≤ 10 nΩ·cm^2) as the temperature dropped below 7 K. In particular, at 4 K the resistivity of joints 8, 9 and 10 decreased to below our (low current) detection limit of ~ 5 nΩ·cm^2. It is well-known that the oxygen content of REBCO affects its critical temperature. It has been reported that the bulk room-temperature resistivity of REBCO films with thickness of 0.6 μm starts to increase after being annealed in air at temperatures above 200 °C for 30 minutes [54] which implies that oxygen is sufficiently mobile to leave the tape at temperatures relevant for solders. A thin (~ 1.5 nm) oxygen deficient REBCO layer at the REBCO/Ag interface is probably the origin of the interfacial resistivity observed in the as-supplied tapes and measured using the $In_{52}Sn_{48}$ joints [55]. However, although the high soldering temperature of 250 °C for the $Pb_{38}Sn_{62}$ joints may often simply degrade the interface by deoxygenating the surface or by promoting delamination if the duration of soldering time was long enough, it is also possible that some oxygen might be able to diffuse into the interface from the bulk and increase both the local oxygen content and local critical temperature [56] leading to the very low resistivity (i.e. low R_i) at $T \leq 6$ K. The relatively high mobility of oxygen at the melting point of commonly used solders provides a straightforward explanation for some of the large variation of R_J found here for $Pb_{38}Sn_{62}$ joints and also found in the literature. We also note the possibility that if the copper

and silver layers are very high purity, proximity coupling between the solder and the REBCO may explain the very low joint resistivity measured at the lowest temperatures [57]. The resistivity of most $Pb_{38}Sn_{62}$ soldered joints (except joint 11) continued to decrease as temperature dropped below the transition temperature of the solder but only one $In_{52}Sn_{48}$ soldered joint (joint 5) showed such behaviour. This complex behaviour might be explained if the proximity effect in $Pb_{38}Sn_{62}$ soldered joints is stronger than in $In_{52}Sn_{48}$ soldered joints, a proposition that can only be tested and quantitative analysis made, with more information about the fundamental superconducting properties of these solders.

5.2. *High current measurements*

Critical current (I_c) measurements were conducted with the sample in direct contact with either liquid nitrogen (77 K) or helium (4.2 K) and in applied magnetic fields up to 12 T. The resistivity of some samples was measured at 4.2 K in magnetic fields up to 9 T in a 40 mm bore horizontal split-pair superconducting magnet at different angles between the field and the tape surface. The voltage (V) across the joints was measured using a nanovolt amplifier and a digital voltmeter while slowly increasing the current (I) through the joint [58]. The electric field (E) criterion used for I_c was 100 μVm^{-1} and the index of transition or n-value was calculated using the power-law expression $E \propto I^n$ with E in the range 100 - 1000 μVm^{-1} [59].Typical voltage-current (V-I) traces taken in zero field at 77 K are shown in Figure 13. When I was much smaller than I_c , the voltage across a soldered joint increased linearly with I, reflecting the resistive nature of the joint. When I was close to I_c an additional V-I power law behavior from the tape is observed, predominantly associated with the (single) tape regions within the voltage taps but outside the joint. The resulting V-I relationship can be written as

$$V = IR + V_c(I/I_c)^n, \qquad 5.2$$

where R is the joint resistance ($R = R_J/\text{Area of the joint}$), n is known as the index or the n-value of the superconductor and V_c is the voltage referenced to the 100 μV/m E-field criterion. As shown in the Figure 13, I_c and the n-value across the joint or along a single CC were similar. These results demonstrate that the resistance of the joint is not dependent on the current and that the REBCO layers in the CCs were not damaged during the fabricating process.

V-I traces at different applied magnetic fields (*B*) at 4.2 K for an $In_{52}Sn_{48}$ soldered joint are plotted in Figure 14. At zero applied field, the *V-I* trace was linear up to 120 A consistent with the $In_{52}Sn_{48}$ solder remaining superconducting and $R_J(0)$ equaling the interfacial resistivity (~ 24 nΩ·cm^2 – consistent with resistivity measurements). There was the expected increase in the resistive slope of the *V-I* traces when the applied field was increased from 0 T to 2 T although the resistance is hysteretic in this field range. The inset to Figure 14 shows the field dependence of the joint resistivity, derived from the high current data in decreasing fields, which has very little field dependence at fields down to 1 T.

The field dependence at 4.2 K of R_J for an $In_{52}Sn_{48}$ and a $Pb_{38}Sn_{62}$ soldered joints is plotted for different orientations of the joints with respect to the field in Figure 15 and Figure 16 respectively. As shown in the figures, R_J of these joints has zero or very weak dependence on both the magnitude and direction of the applied magnetic field. These results are consistent with most of the literature findings [7, 36] although there is a report of a very large field dependence in R_J [37]. However, in that report [37], R_J of all the samples that show large magnetoresistance at 77 K is higher than 100 nΩ·cm^2 which may suggest it is specific to damaged samples or those with high joint resistivity.

5.3. *Heating inside joints*

A miniature copper/constantan Type T thermocouple was inserted into the centre of the solder of a $In_{52}Sn_{48}$ joint with a 410 μm thick layer of solder and used to monitor the increase in temperature as a function of a slowly-increasing current (*I*) through the joint. As shown in Figure 17 the joint temperature initially varied roughly as $I^{1.7}$ up to a few hundred mK, which is similar to I^2 in Equation 4.11. Above I_c, the temperature increased much more rapidly. The experimental data are consistent with FEA results, that show the temperature inside typical (~ 25 μm thick solder) joints will increase by less than a few hundred mK at 77 K at currents below I_c.

6. The Cryogenic cost of Demountable Joints in Fusion Applications

Resistive demountable joints produce an additional cryogenic heat load cost that we estimate for fusion applications as follows: we expect the R_J of a soldered joint for two REBCO CCs to be well below 50 nΩ·cm^2 (c.f. Figure 11 and Figure 12), with a resistance for a single joint below 25 nΩ assuming the overlap area of the CCs is > 2 cm^2. If we take the ITER TF coils as an example, each cable carries 68 KA and has 900 strands. There are 134 turns in each TF coil and 18 coils. This gives about 4½ million joints in the TF coils generating about 600 W at the operating temperature. In ITER there is a cryogenic requirement of ~ 50 kW so the additional cost from the demountable joints is small - below 1 % of the total cryogenic cost. Commercial fusion tokamaks will require magnets that can be demounted quickly. We have not yet ruled out a practical route for making and breaking many joints in parallel. However it seems probable that demountable magnets will include demountable cables that include several million component (non-demountable) joints. The cable-cable joints (not considered in this paper) will bring an additional cryogenic cost dependent on the demountable cable design but we expect it to be small because it may for example be pressed copper which has a much lower resistivity than solder (cf Table 3). Developing cable-cable measurements and design is part of our future work, but we expect that the joints necessary to enable demountable magnets in fusion applications should only add a few percent to the total cryogenic cost.

7. Discussion and future work

Table 2 shows that there are many alloys that can be used as solders with melting points lower than room temperature. Such low melting points enable a different process for mounting or demounting joints soldered by these alloys. One can sandwich a thin layer of one of these alloys between two REBCO coated conductor tapes or the solder can simply be painted onto the superconducting tape without the need to apply any heat at room temperature. At low temperatures the alloy becomes solid and connects the two tapes together mechanically and electrically. At room temperature such joints can be demounted easily because the joint solder becomes liquid. A joint between two YBCO tapes was fabricated using gallinstan (see Table 2) which has a viscosity more than twice that of water. The joint resistivity was 45 nΩ·cm^2 at 77 K, comparable to that of our $Pb_{38}Sn_{62}$ soldered joints (see Figure 12) and with a thickness of the gallinstan layer estimated to be ~30 μm. It is expected that this thickness can be reduced by half by applying higher pressure at the joint and achieve a joint resistivity lower than those achieved

using $Pb_{38}Sn_{62}$ solders. Table 7 shows that indium is much more expensive than the other constituent metals for the low temperature solders listed in Table 2 and so may need to be avoided for reasons of cost. In light of this we have also made joints with $Bi_{52.5}Pb_{32}Sn_{15.5}$ solder and achieved a joint resistivity of 63 $n\Omega \cdot cm^2$ at 77 K. The soldering temperature was 150 °C. Further work is needed to identify the best choice of solder for fabricating joints for fusion applications, to characterise the mechanical strength of these joints and to develop guidelines for developing the best designs for demountable cables.

8. Conclusions

The fundamental properties of soldered joints of two REBCO CCs have been investigated using SEM studies, numerical analysis, resistivity and critical current measurements. Numerical results show that resistive current across a joint is broadly uniform and confined within the joint. The temperature at the centre of a soldered joint was found to be less than a few hundred mK when operating at 100 A. Our resistivity and critical current data showed that at temperatures between ~ 7 K and ~ 90 K, the joint resistivity of an $In_{52}Sn_{48}$ soldered joint predominately had two sources, the solder layer (~20 - 30 $n\Omega \cdot cm^2$) and the temperature independent interfacial resistivity of the REBCO/Ag interface within the CCs (~25 $n\Omega \cdot cm^2$) and can be described using a simple mathematical equation. The magnetic field dependence of the joint resistivity was very weak and confirmed to be independent of the angle between the surface of the tapes and the magnetic field. We propose that increased delamination in REBCO tapes and increased mobility of the oxygen in the REBCO at higher temperatures provide an explanation for the large variation of R_J in $Pb_{38}Sn_{62}$ soldered joints we have found here and found in the literature. This work shows that HTS conductors that have both high critical current density and low interfacial resistivity may provide a practical route for demountable magnets inside an HTS commercial tokamak and demonstrates that demountable joints need only add just a few percent to the total cryogenic load in a commercial fusion tokamak.

Acknowledgements

We would like to thank: Matthew Plumb, Robert Edge, Stephen Webster and Tom Lee for help with calculations; Tom Hudson, Simone Smith, Prapaiwan Sunwong, Andrea Dawson, Victoria Stutt, Tom Todd and Mark J. Raine for help with and discussions about joint fabrication and

cryogenic high-field measurements; Steve Lishman and Andrew Davies for building the cryogenic probes; and Budhika Mendis and Leon Bowen for help with the electron microscopy. This work was funded by the RCUK Energy Programme under grant EP/I501045. Figure 1 is courtesy of SuperPower, Inc., a Furukawa Company, copyright 2015. The data in this paper are available at http://dx.doi.org/10.15128/gh93gz491.

Tables

Table 1: Specifications for the SuperPower Inc. IBAD-MOCVD REBCO coated-conductor superconducting tapes used in this study [40].

Model number	SCS4050
Average I_c at 77 K in self-magnetic field	98 A
Average n-value at 77 K	30
Width	3.99 mm
Overall Thickness	0.095 mm

Table 2: Resistivity at room temperature and 77 K, measured in Durham, and melting points, from the literature, [60, 61] of some low-temperature solders and their constituent metals.

Solder/constituent Metal	Resistivity at room temperature(Ω·m)	Resistivity at 77 K (Ω·m)	Liquids (°C)	Solidus (°C)	$\frac{\rho(Room\ Temperature)}{\rho(77\ K)}$
In	1.02×10^{-7}	1.79×10^{-8}	156.6	156.6	5.7
Sn	1.46×10^{-7}	2.59×10^{-8}	231.9	231.9	5.64
Ga	3.03×10^{-7}	5.61×10^{-8}	29.8	29.8	5.41
Pb	2.45×10^{-7}	5.43×10^{-8}	327.5	327.5	4.51
Bi	1.80×10^{-6}	1.18×10^{-6}	271.4	271.4	1.53
Commercial $Pb_{40}Sn_{60}$	1.64×10^{-7}	3.71×10^{-8}	183	190	4.42
$Pb_{38}Sn_{62}$	1.81×10^{-7}	4.10×10^{-8}	183	183	4.41
$In_{52}Sn_{48}$	2.60×10^{-7}	1.25×10^{-7}	118	118	2.08
$Bi_{50}Pb_{26.7}Sn_{13.3}Cd_{10}$ (Wood's metal)	5.24×10^{-7}	1.93×10^{-7}	70	70	2.71
$Pb_{38}Bi_{37}Sn_{25}$	5.80×10^{-7}	3.08×10^{-7}	127	93	1.88
$Bi_{52.5}Pb_{32}Sn_{15.5}$	7.22×10^{-7}	3.60×10^{-7}	95	95	2.01
$In_{66.3}Bi_{33.7}$	8.29×10^{-7}	3.91×10^{-7}	72	72	2.12
$Bi_{57}In_{26}Sn_{17}$	9.08×10^{-7}	4.13×10^{-7}	79	79	2.20
$Bi_{44.7}Pb_{22.6}In_{19.1}Sn_{8.3}Cd_{5.3}$ (Cerrolow 117)	6.94×10^{-7}	4.32×10^{-7}	47	47	1.61
$Bi_{58}Pb_{42}$	1.11×10^{-6}	6.69×10^{-7}	126	124	1.66
$Bi_{55}Pb_{44}Sn_{1}$	1.28×10^{-6}	7.45×10^{-7}	120	117	1.72
Alloys – liquid at room temperature					
$Ga_{66.5}In_{20.5}Sn_{13}$	2.98×10^{-7}	6.94×10^{-8}	10.7	10.7	4.29
$Ga_{75.5}In_{24.5}$	2.91×10^{-7}	7.02×10^{-8}	15.7	15.7	4.15
$Ga_{68.5}In_{21.5}Sn_{10}$ (Gallinstan)	2.68×10^{-7}	7.17×10^{-8}	-19	-19	3.74

Table 3: Electrical and thermal conductivity materials properties of the components of a soldered joint at different temperatures. ‡These values were obtained from resistivity measurements on solders in Durham. The layer thicknesses cited for the tape are taken from SuperPower Inc. The properties of commercial $Pb_{40}Sn_{60}$ solder are also included for comparison.

Material	Electrical Conductivity (10^8 Sm^{-1})	Thermal Conductivity (W m^{-1} K^{-1})	Layer Thickness (μm)
Copper (OFHC) RRR = 100 [62, 63]	0.59 (295K); 4.76 (77 K); ~ 59 (4.2 K).	397 (295K); 547 (77 K); 642 (4.0 K).	20
HASTELLOY® C-276 [64]	0.008 (77 K); 0.008 (4.2 K).	~ 7.8 (77 K); ~ 0.7 (4.2 K).	50
$Pb_{38}Sn_{62}$ (wt. %) solder	0.056 (295K) ‡; 0.24 (77 K) ‡; 1.12 (10 K) ‡; superconducting (7.0K) ‡.	64 (295 K); 56 (77 K); ~ 42 (10 K) ~ 17 (4.2 K) [62].	10
Commercial $Pb_{40}Sn_{60}$ (wt. %) solder	0.063 (295K) ‡; 0.27 (77 K) ‡; 1.59 (10 K) ‡; superconducting (~6K) ‡.	50 (295 K); 52 (77 K) [65]	N/A
$In_{52}Sn_{48}$ (wt. %) solder	0.038 (295K) ‡; 0.080 (77 K) ‡; 0.11 (10 K) ‡; superconducting (6.2K) ‡.	34 (295 K) [66].	30
REBCO	> 1.10×10^{10}	77 K [67]: ~ 20 (*ab*-plane) ~ 2.3 (*c*-axis)	1
Ag (RRR = 1800) [62, 68]	0.625 (295K); 3.704 (77 K); ~ 1125 (4.2 K).	429 (295K); 479 (77 K); 14700 (4.0 K).	2

Table 4: The cryogenic properties of liquid nitrogen and liquid helium

Property	Liquid nitrogen (77K) [69-72]	Liquid Helium (4.2K) [73]
Viscosity (η)	1.58×10^{-4} [Pa.s^{-1}]	3.244×10^{-6} [Pa.s^{-1}]
Mass density (ρ_m)	808 [kg.m^{-3}]	125.407 [kg.m^{-3}]
Kinematic Viscosity (ν)	1.955×10^{-7} [m^2.s^{-3}]	2.587×10^{-8} [m^2.s^{-1}]
Thermal Expansivity (β)	0.00753 [K^{-1}]	0.153 [K^{-1}]
Thermal Conductivity (κ)	0.138 [W.m^{-1}.K^{-1}]	0.01994 [W.m^{-1}.K^{-1}]
Specific Heat Capacity (c_p)	2.042×10^{3} [J.kg^{-1}.K^{-1}]	4.467×10^{3} [J.kg^{-1}.K^{-1}]
Thermal Diffusivity (α)	8.36×10^{-8} [m^2.s^{-1}]	3.55×10^{-8} [m^2.s^{-1}]

Table 5: Comparison of the electrical and thermal properties of an idealised soldered joint and a multilayered joint calculated using analytic and FEA methods. The idealized soldered joint consists of two slabs of thermally insulating superconductor connected by a cylinder of solder as shown in Figure 7. The multilayered joint structure is shown in Figure 6. J and E are the current density and the electric field in the solder respectively. ΔT is the temperature difference between the centre of the joint (hottest) and the surrounding cryogen (77 K) when 100 A flows through the $Pb_{38}Sn_{62}$ joint. The analytic values are derived using Eqn 4.11 for the idealized joint and Eqn. 4.12 for the multilayered joint.

	Method	J (10^6Am^{-2})	E (Vm^{-1})	h (Wm^{-2})	ΔT (mK)
Idealised Joint	Analytic (77 K)	6.25	0.297	6056	389
	FEA (77 K)	6.28	0.299	6052	384
Multilayered joint	Analytic Approx. (77 K)	6.25	0.297	205.5	24.7
	FEA (77 K)	6.14	0.292	207.0	20.7

Table 6: The critical temperature and critical field of some superconducting elements and alloys used to make resistive superconducting joints. Pb, Sn and In are Type I superconductors – the thermodynamic critical field is quoted. $Pb_{38}Sn_{62}$ and $In_{52}Sn_{48}$ [74] are Type II superconductors – the upper critical field ($B_{c2}(0)$) is quoted. ‡These values were obtained from resistivity measurements on alloys/solders in Durham. B_{c2} was taken at the onset of the transition.

Material	Critical Temperature (K)	Critical field (mT)
Pb	7.20	75
Sn	3.72	30
In	3.41	28
$Pb_{38}Sn_{62}$	7.3‡	300‡
$In_{52}Sn_{48}$	6.4‡	340‡

Table 7: Approximate prices for the high purity (≥ 99.9 %) constituent metals of the solders shown in **Table 2**. In the table, prices for high purity silver and gold are also shown for comparison.

Metal	Form	Purity (%)	Price (£/gram)
Tin	Ingots	99.9	0.13
Lead	Rods	99.99	0.15
Bismuth	Pellets	99.99	0.64
Gallium	Ingots	99.99	0.66
Silver	Rods	99.99	0.99
Cadmium	Sheets	99.95	1.14
Indium	Ingots	99.99	2.08
Gold	Sheet	99.99	73.2

Figures

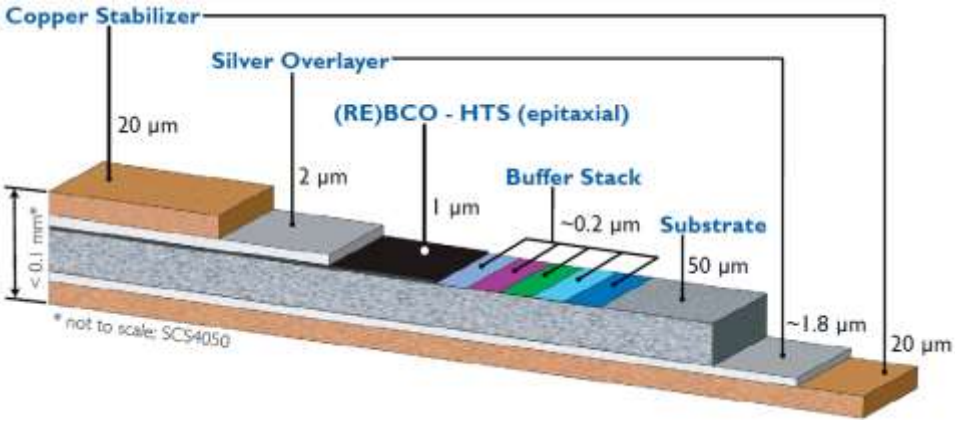

Figure 1: Multilayer structure of a SuperPower IBAD-MOCVD REBCO coated-conductor superconducting tape [40].

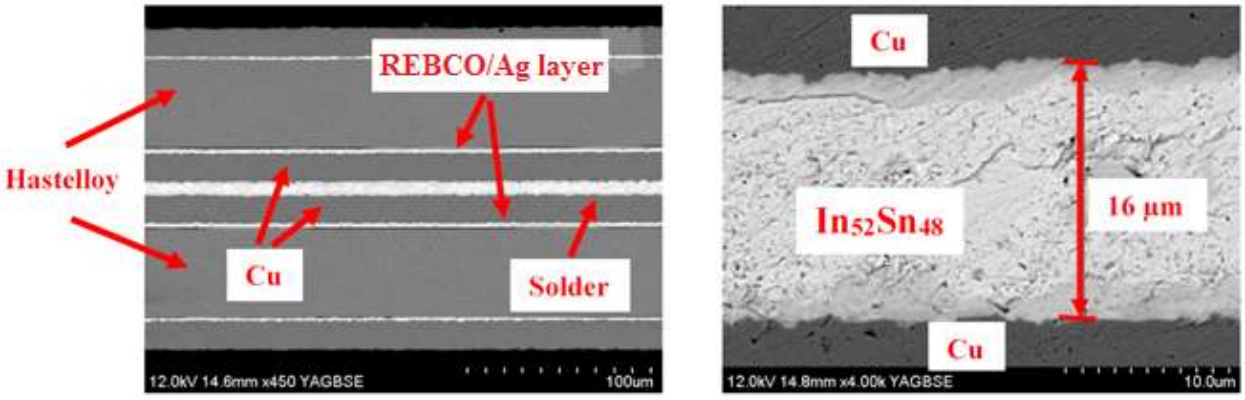

Figure 2: SEM images of a soldered joint made using two SuperPower REBCO tapes and $In_{52}Sn_{48}$ solder between them.

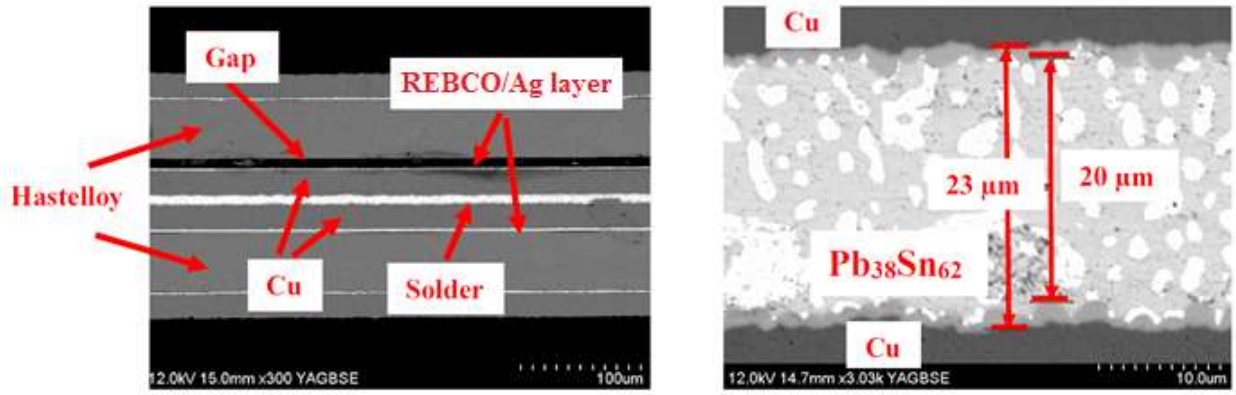

Figure 3: SEM images of a soldered joint made using two SuperPower REBCO tapes and $Pb_{38}Sn_{62}$ solder between them. A gap is present between the REBCO/Buffer layers and the Hastelloy layer in this joint. This tendency for delamination may explain why some $Pb_{38}Sn_{62}$ joints can have anomalously large interfacial resistivities after handling.

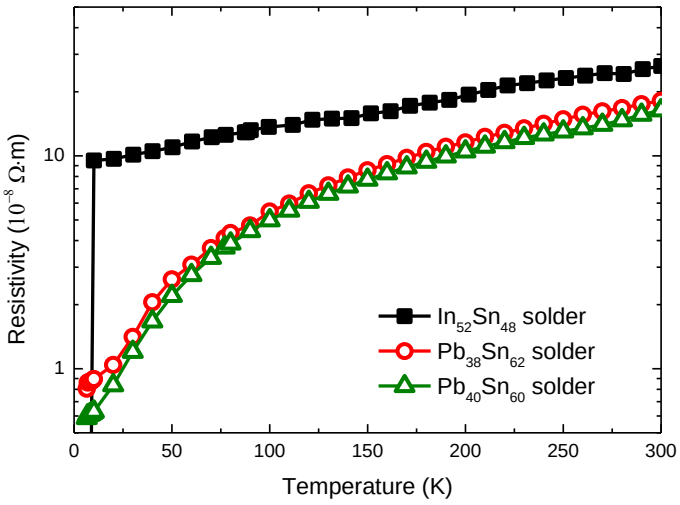

Figure 4: Resistivity as a function of temperature for $In_{52}Sn_{48}$, $Pb_{38}Sn_{62}$ and $Pb_{40}Sn_{60}$ solders at temperatures below 300 K. $In_{52}Sn_{48}$ and $Pb_{38}Sn_{62}$ were fabricated in Durham and $Pb_{40}Sn_{60}$ was purchased from a commercial supplier.

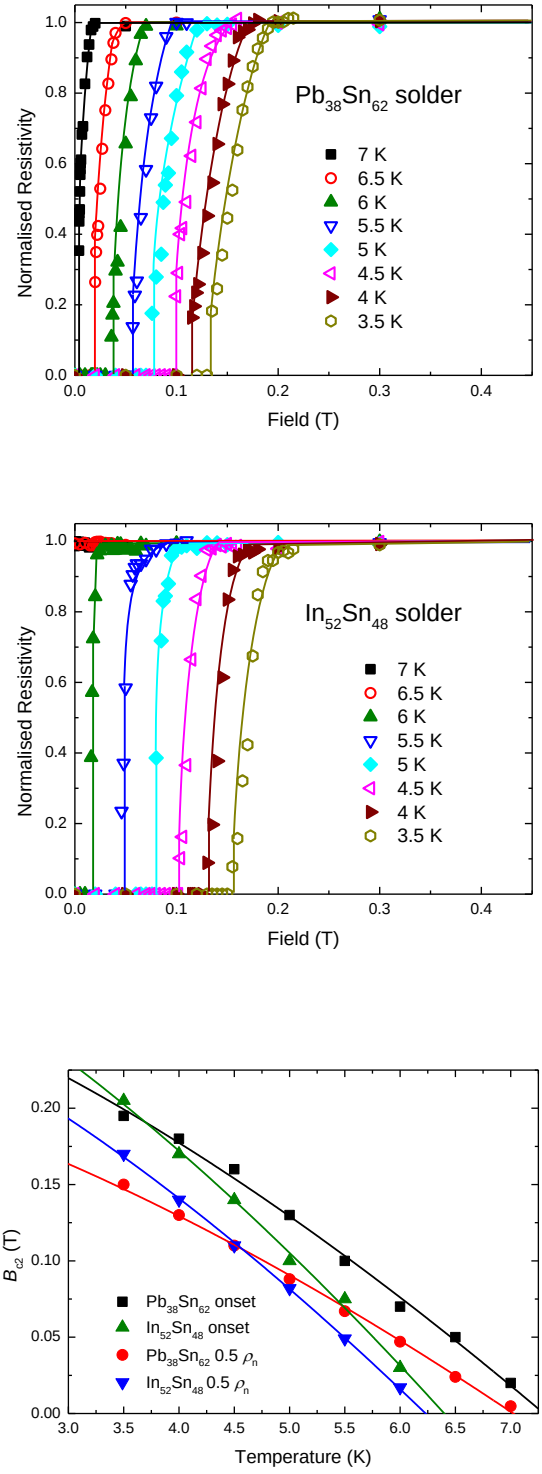

Figure 5: The normalised resistivity of $Pb_{38}Sn_{62}$ (upper) and $In_{52}Sn_{48}$ (middle) solders as a function of (increasing) applied magnetic fields at low temperatures. Lines are guide to the eye. Lower: Upper critical field (B_{c2}) of $Pb_{38}Sn_{62}$ and $In_{52}Sn_{48}$ solders as a function of temperature. B_{c2} defined using two criteria: at the onset of transition (solid triangles and squares) and when the solder resistance equalled half of the normal state value (solid down triangles and circles). Curves are fitted using the W-H-H equation [75].

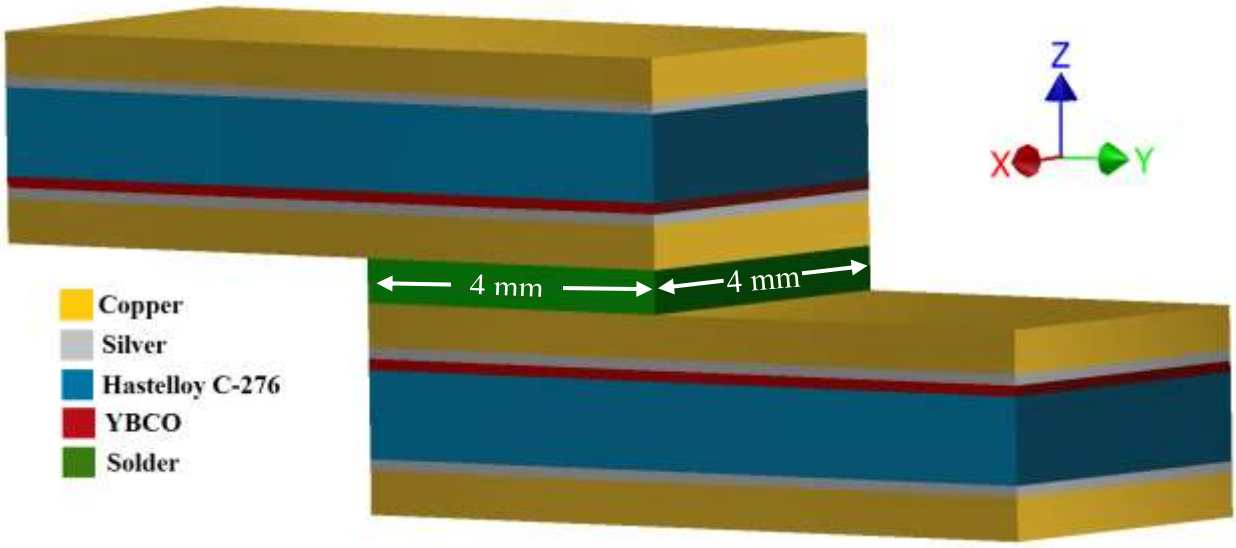

Figure 6: The soldered joint structure used to calculate the electrical and thermal properties of the joint. The very thin buffer layers in the tapes are not included in the structure used to model the joint. The thicknesses of the different layers are not to the scale and are given in Table 3.

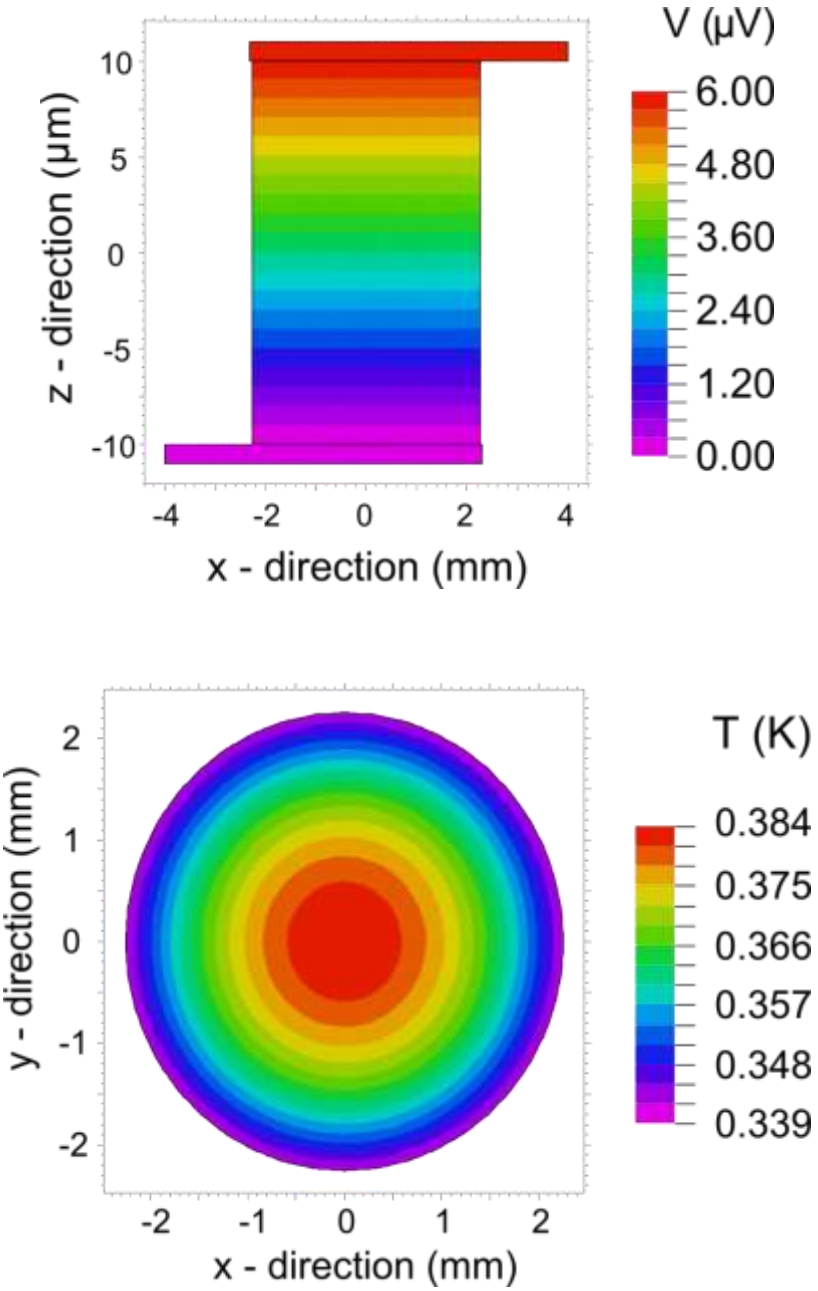

Figure 7: The voltage profile and temperature profile through an idealised soldered joint. The joint consists of a cylinder of solder, 20 μm thick with a radius of $4/\sqrt{\pi}$ mm, which connects two 1 μm thick, 4.6 mm wide, thermally insulating superconducting slabs. The voltage is generated by injecting 100 A into the top right-hand side of the upper superconducting slab which passes through the joint and flows to ground through the bottom superconducting slab. The solder has the properties of $Pb_{38}Sn_{62}$ operating at 77 K. Upper: The voltage profile is a cutaway through the centre of the joint along its length. The gradient in the voltage (i.e. the electric field) is uniform within the solder (i.e. y = 0). Lower: The temperature profile is a slice through the centre of the joint (i.e. z = 0). The temperature gradient throughout the slice is radial. Heat conduction into the cryogen takes account of buoyancy or equivalently the direction of gravity which in this figure is down the axis of the solder.

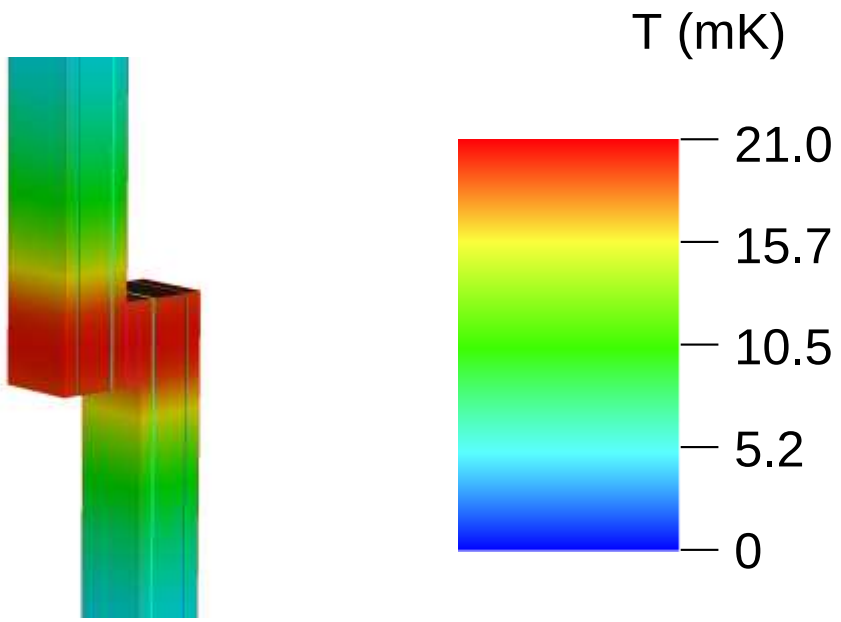

Figure 8: A three-dimensional visualization of the temperature profile through a soldered joint which is operating at 77 K and conducts 100 A. The joint consists of a cuboid of $Pb_{38}Sn_{62}$ solder, 20 μm thick with 4 mm × 4 mm sides, between two multilayered REBCO superconducting tapes which each consist of Cu/Ag/Hastelloy/REBCO/Ag/Cu. The thicknesses of the layers are given in Table 3. Heat conduction into the cryogen takes account of buoyancy or equivalently the direction of gravity which in this figure is taken to be in the long direction of the tapes, broadly down the page.

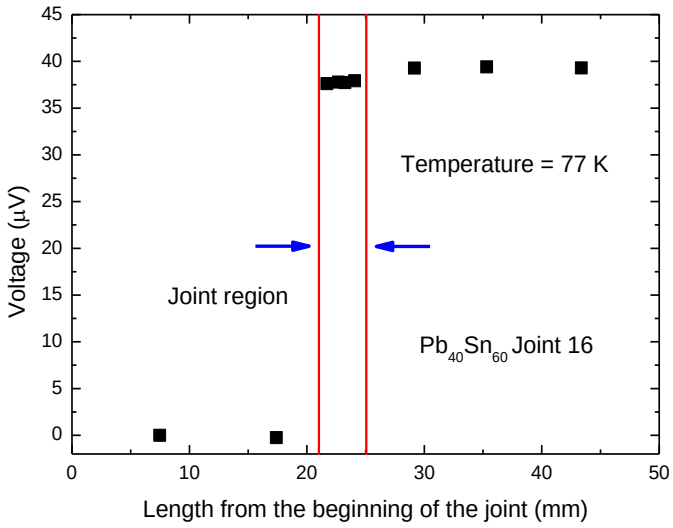

Figure 9: The voltage across a soldered joint at 77 K with respect to a tap about 21 mm from the joint on the grounded REBCO tape, when carrying 80 A. The joint consisted of two REBCO tapes joined by a cuboid of $Pb_{40}Sn_{60}$ solder of joint area 4 mm × 4 mm and nominal thickness of ~ 25 microns. Generic behaviour is observed where the voltage differences between two taps that are both on either one of the component REBCO tapes is zero but the total voltage across the joint is observed between any two taps that are on the different tapes.

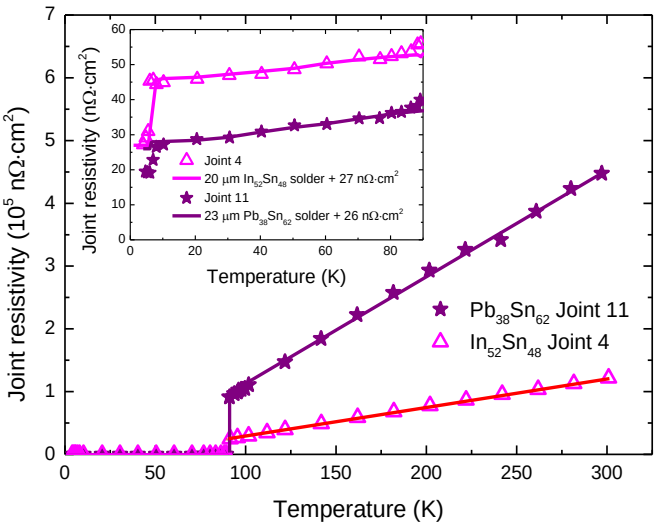

Figure 10: Joint resistivity as a function of temperature for two soldered joints made using $In_{52}Sn_{48}$ and $Pb_{38}Sn_{62}$ solders. The resistivity of the joints at 40 K were 47 nΩ·cm^2 (resistance ~ 300 nΩ) and 31 nΩ·cm^2 (resistance ~ 210 nΩ) for the $In_{52}Sn_{48}$ and $Pb_{38}Sn_{62}$ joints respectively. Measurements were made in zero applied field.

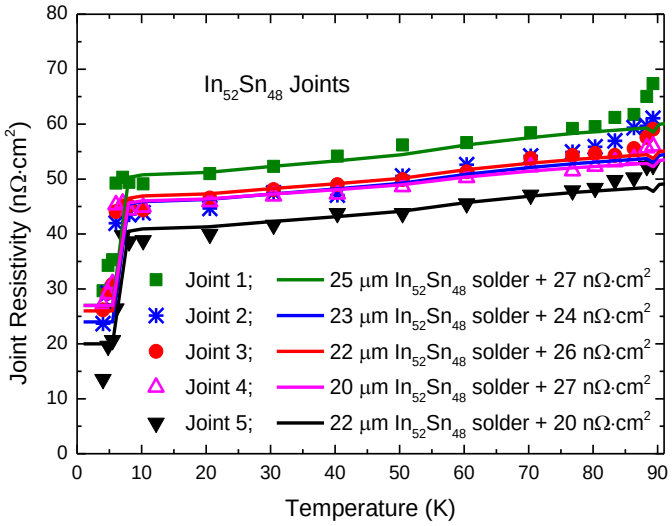

Figure 11: Joint resistivity versus temperature for five joints fabricated using $In_{52}Sn_{48}$ solder. The soldered joint area for Joints 1 to 5 were 4 mm × 3.9 mm, 4 mm × 2.7 mm, 4 mm × 3.9 mm, 4 mm × 4 mm and 4 mm × 2.8 mm respectively. Lines are fits using equation 5.13 which uses the thickness of the solder as a free parameter and assumes the interfacial resistivity is temperature independent. Interfacial resistivity was found to be in the range of 20 to 27 $n\Omega \cdot cm^2$. Measurements were made in zero applied field.

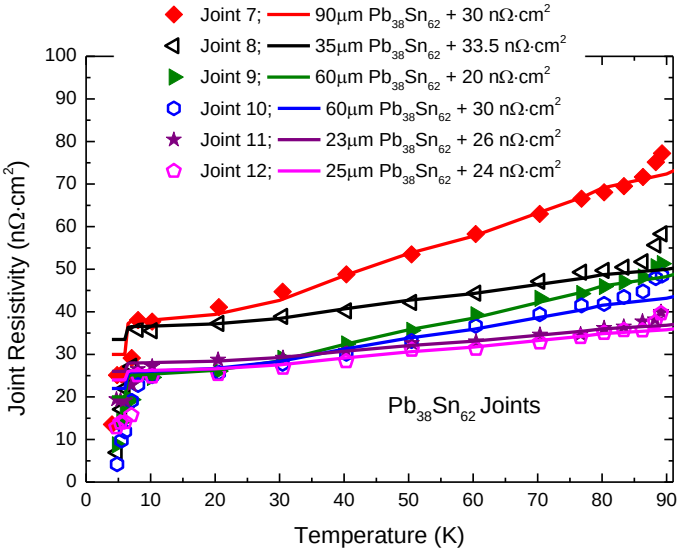

Figure 12: Joint resistivity as a function of temperature for six joints fabricated using $Pb_{38}Sn_{62}$ solder. The soldered joint areas were 4 mm × 3.3 mm, 4 mm × 3.5 mm, 4 mm × 3.8 mm, 4 mm × 3.9 mm, 4 mm × 3.6 mm and 4 mm × 3.8 mm for joints 7 to 12 respectively. Lines are fits using equation 5.13 which uses the thickness of the solder and the interfacial resistivity as free parameters. The interfacial resistivity is also assumed to be temperature independent. Joints 11 and 12 were found to have an interfacial resistivity of 25 $n\Omega \cdot cm^2$. However, the resistivity of other joints cannot be described properly using equation 5.13 because the derived thicknesses of the solder (which microscopy shows in 25 μm) are not physically large. Measurements were made in zero applied field

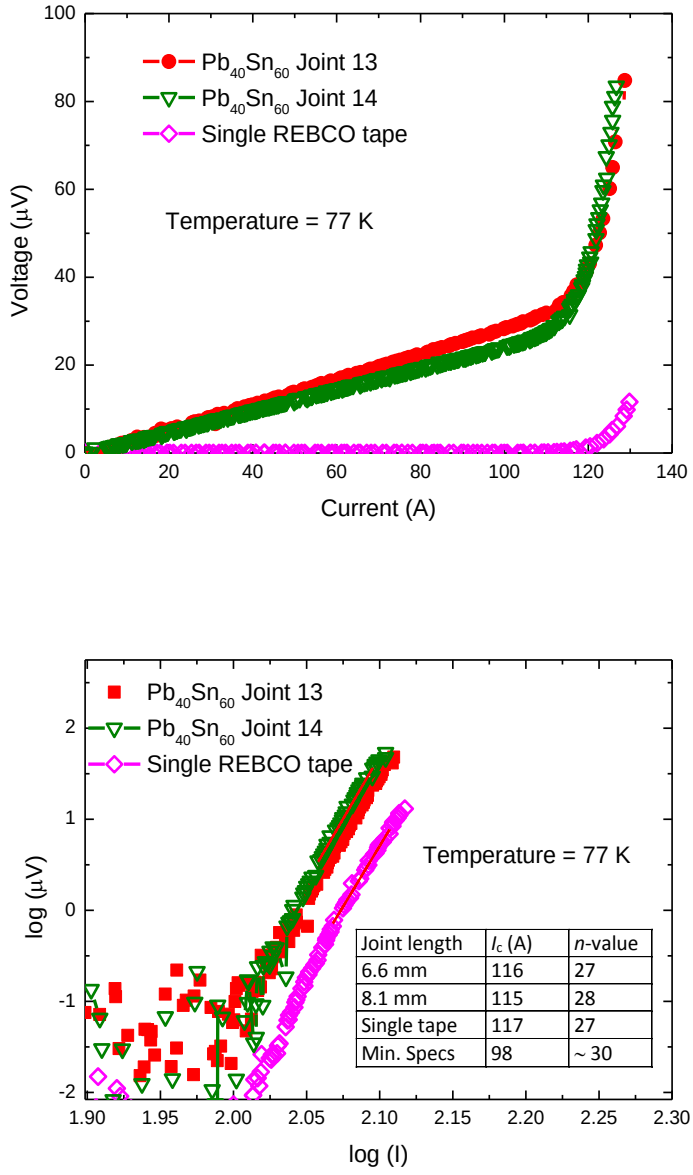

Figure 13: Voltage-Current (*V-I*) traces for two soldered joints and a single REBCO tape. Upper: The raw *V-I* data. Lower: Data replotted with the resistive contribution from the joints removed. For Joint 13 the solder used was $Pb_{40}Sn_{60}$ and the soldered joint area was 4 mm × 6.6 mm. For Joint 14 the soldered joint area was 4 mm × 8.1 mm. In both joints the expected nominal thickness was ~ 25 microns. The critical current and the *n*-value are similar in the two joints and the tape. Measurements were made in zero applied field.

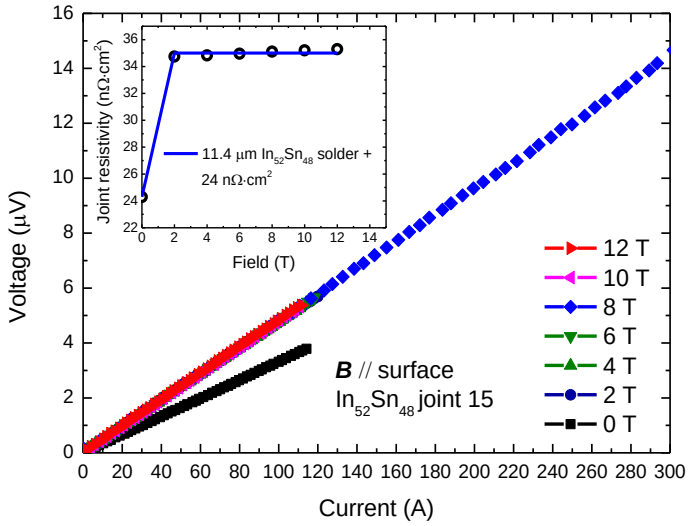

Figure 14: Voltage-Current (*V-I*) traces at 4.2 K for a joint fabricated using $In_{52}Sn_{48}$ solder as a function of the field applied parallel to the broad surface of the tape. Most *V-I* traces were taken up to 120 A, although data up to 300 A at 8 T are also shown. Inset: Joint resistivity of the $In_{52}Sn_{48}$ joint at 4.2 K as a function of applied field. The line is a fit using the assumption that joint resistivity is solely due to an 11.4 micron thick $In_{52}Sn_{48}$ solder layer with a temperature independent interfacial resistivity of 24 $n\Omega \cdot cm^2$.

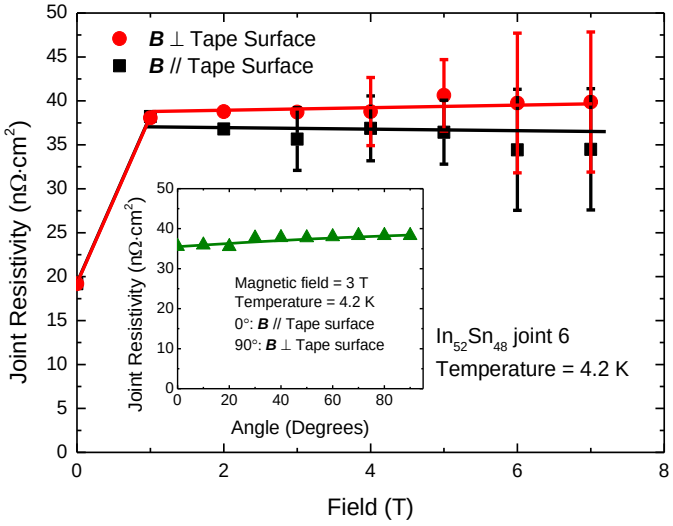

Figure 15: Magnetoresistance of the joint resistivity at 4.2 K as a function of applied magnetic field. The solder used was $In_{52}Sn_{48}$ and the soldered joint area was 4 mm × 18.6 mm and an expected nominal thickness of ~ 25 microns. Inset shows the joint resistivity as a function of the angle between the orientation of the tape and the direction of the applied field at 3 T and 4.2 K.

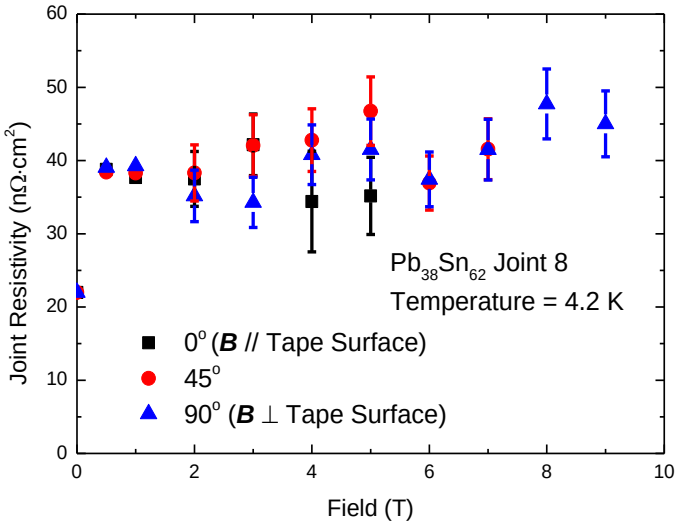

Figure 16: Joint resistivity of soldered joints at 4.2 K as a function of field at different orientations of the tape with respect to the applied field. The solder used was $Pb_{38}Sn_{62}$ and the soldered joint area was 4 mm × 3.5 mm and an expected nominal thickness of ~ 25 microns. The angles are those between the applied field and the surface of the tape.

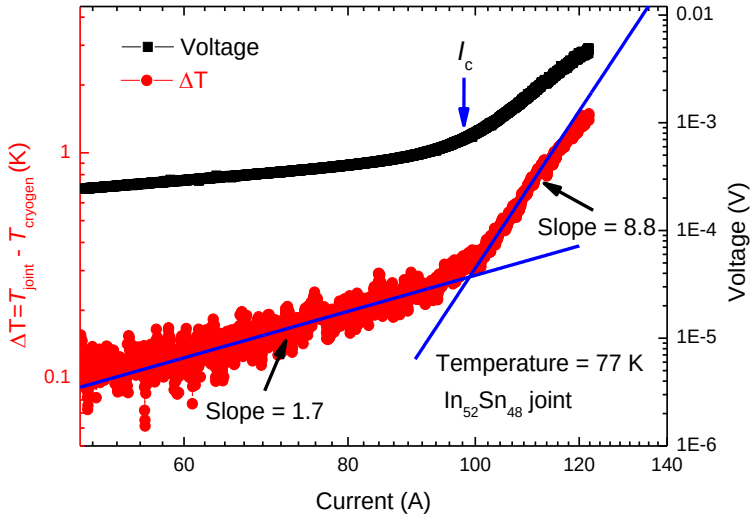

Figure 17: The voltage across a joint and the temperature difference between the centre of the joint and the cryogen, as a function of current through the joint. The joint consisted of two REBCO tapes joined by a cuboid of $In_{52}Sn_{48}$ solder of joint area dimensions 4 mm × 4.8 mm and thickness of 0.41 mm. Measurements were made in zero applied field.

REFERENCES

[1] V. Selvamanickam, A. Xu, Y. Liu, N.D. Khatri, C. Lei, Y. Chen, E. Galstyan, G. Majkic, Correlation between in-field critical currents in Zr-added (Gd,Y)$Ba_2Cu_3O_x$ superconducting tapes at 30 K and 77 K, Supercond. Sci. and Technol., 27 (2014) 055010.
[2] T.S. Lee, I. Jenkins, E. Surrey, D.P. Hampshire, Optimal design of a toroidal field magnet system and cost of electricity implications for a tokamak using high temperature superconductors Fusion Engineering and Design, 98-99 (2015) 1072–1075.
[3] Z.S. Hartwig, C.B. Haakonsen, R.T. Mumgaard, L. Bromberg, An initial study of demountable high-temperature superconducting toroidal field magnets for the Vulcan tokamak conceptual design, Fus. Eng. and Design, 87 (2012) 201.
[4] A. Sagara, T. Goto, J. Miyazawa, N. Yanagi, T. Tanaka, H. Tamura, R. Sakamoto, M. Tanaka, Design activities on helical DEMO reactor FFHR-d1, Fusion Engineering and Design, 87 (2012) 594.
[5] A.M. Garofalo, V.S. Chan, J.M. Canik, M.E. Sawan, M. Choi, D.A. Humphreys, L.L. Lao, R. Prater, P.C. Stangeby, H.E. St. John, T.S. Taylor, A.D. Turnbull, C.P.C. Wong, Progress in the physics basis of a Fusion Nuclear Science Facility based on the Advanced Tokamak concept, Nucl. Fusion, 54 (2014) 073015.
[6] B.G. Hong, Y.S. Hwang, J.S. Kang, D.W. Lee, H.G. Joo, M. Ono, Conceptual design study of a superconducting spherical tokamak reactor with a self-consistent system analysis code, Nucl. Fusion, 51 (2011) 113013.
[7] J. Lu, K. Han, W.R. Sheppard, Y.L. Viouchkov, K.W. Pickard, W.D. Markiewicz, Lap joint resistance of YBCO coated conductors, IEEE Trans. Appl. Supercond., 21 (2011) 3009.
[8] Y. Kim, J. Bascunan, T. Lecrevisse, S. Hahn, J. Voccio, D.K. Park, Y. Iwasa, YBCO and Bi2223 Coils for High Field LTS/HTS NMR Magnets: HTS-HTS Joint Resistivity, IEEE Trans. Appl. Supercond., 23 (2013) 6800704.
[9] G. Casini, Fusion technology (Report on the 13th Symposium, Varese, Italy 24–28 September 1984), Nucl. Fusion, 25 (1984) 633.
[10] I. GROUP, International tokamak reactor - phase two A, part III, Nucl. Fusion, 28 (1988) 711.
[11] J.L. Luxon, A design retrospective of the DIII-D tokamak, Nucl. Fusion, 42 (2002) 614.
[12] J.E. Menard, L. Bromberg, T. Brown, T. Burgess, D. Dix, L. El-Guebaly, T. Gerrity, R.J. Goldston, R.J. Hawryluk, R. Kastner, C. Kessel, S. Malang, J. Minervini, G.H. Neilson, C.L. Neumeyer, S. Prager, M. Sawan, J. Sheffield, A. Sternlieb, L. Waganer, D. Whyte, M. Zarnstorff, Prospects for pilot plants based on the tokamak, spherical tokamak and stellarator, Nucl. Fusion, 51 (2011) 103014.
[13] J.R. Powell, S.Y. Hsieh, G. Danby, P. Bezler, D. Gardner, C. Laverick, M. Finkelman, T. Brown, J. Bundy, T. Balderes, I. Zatz, R. Verzera, R. Herbermann, DEALS: a demountable superconducting magnet system for fusion reactors, Cryogenics, 20 (1980) 59 - 74.
[14] K. UO, O. Motojima, T. Horiuchi, Y. Monju, M. Hamada, Contact Resistance of Demountable Multi-pin Joint for Superconducting Helical Coil, Proceedings of the Fourteenth Symposium on Fusion Technology, (1986) 1727-1732.
[15] H. Hashizume, S. Ito, Design prospect of remountable high-temperature superconducting magnet, Fusion Engineering and Design, 89 (2014) 2241-2245.
[16] M. Sborchia, E. Barbero Soto, R. Batista, B. Bellesia, A. Bonito Oliva, E. Boter Rebollo, T. Boutboul, B. E, J. Caballero, M. Comelis, J. Fanthome, R. Harrison, M. Losasso, A. Portone, H. Rajainmaki, P. Readman,

P. Valente, Overview of ITER Magnet System and European Contribution, IEEE/NPSS 24th Symposium on Fusion Engineering, (2011) S03D-l.
[17] L. Zani, P. Barabaschi, P. Bruzzone, D. Ciazynski, P. Decool, B. Lacroix, M. Nannini, B. Stepanov, A. Torre, J.M. Verger, Test and analyses of two TF conductor prototypes for JT-60SA, IEEE Trans. Appl. Supercond., 20 (2010) 451.
[18] G. Rolando, A. Foussat, J. Knaster, Y. Ilin, A. Nijhuis, Performance assessment and optimization of the ITER toroidal field coil joints, Superconductor Sciences and Technology, 26 (2013) 085004.
[19] P. Decool, D. Ciazynski, A. Nobili, S. Parodi, P. Pesenti, A. Bourquard, F. Beaudet, Joints for large superconducting conductors, Fusion Engineering and Design, 58-59 (2001) 123-127.
[20] C. Sborchia, H. Fillunger , R. Maix, E. Salpietro, Progress on R&D and design work for the ITER toroidal field coils, 20th IEEE/NPSS Symposium on Fusion Engineering, (2003) 432.
[21] Y. Lvovsky, E.W. Stautner, T. Zhang, Novel technologies and configurations of superconducting magnets for MRI, Supercond Sci Tech, 26 (2013) 093001.
[22] C.A. Swenson, W.D. Markiewicz, Persistent joint development for high field NMR, IEEE Trans Appl Super, 9 (1999) 185.
[23] Y. Park, M. Lee, H. Ann, Y.H. Choi, H. Lee, A superconducting joint for $GdBa_2Cu_3O_{7-delta}$-coated conductors, NPG Asia Materials, 6 (2014) e98.
[24] K. Kawai, S. Ito, Y. Seino, N. Yanagi, H. Tamura, A. Sagara, H. Hashizume, Optimization of a mechanical bridge joint structure in a stacked HTS conductor, IEEE Trans. Appl. Supercond., 23 (2013) 4801704.
[25] S. Ito, T. Ohinata, L. Bromberg, H. Hashizume, Structure improvement and joint resistance estimation in demountable butt and edge joints of a stacked REBCO conductor within a metal jacket, IEEE Trans. Appl. Supercond., 23 (2013) 4802408.
[26] S. Ito, K. Kawai, Y. Seino, T. Ohinata, Y. Tanno, N. Yanagi, Y. Terazaki, K. Natsume, S. Hamaguchi, H. Noguchi, H. Tamura, T. Mito, A. Sagara, H. Hashizume, Performance of a Mechanical Bridge Joint for 30-kA-Class High-Temperature Superconducting Conductors, IEEE Transaction on applied superconductivity, 24 (2014).
[27] M. Takayasu, L. Chiesa, L. Bromberg, J.V. Minervini, Cabling method for high current conductors made of HTS tapes, IEEE Trans. Appl. Supercond., 21 (2011) 2340.
[28] M. Yagi, S. Mukoyama, T. Mitsuhashi, T. Jung, L. Jin, M. Suzuki, H. Hirata, T. Nomura, R. Nakayama, N. Maesato, T. Okuma, O. Maruyama, The development of 275 kV-3 kA YBCO high-Tc superconducting power cable, Furukawa Review, 43 (2013) 19.
[29] S. Mukoyama, M. Yagi, H. Hirata, M. Suzuki, S. Nagaya, N. Kashima, Y. Shiohara, Development of YBCO high-Tc superconducting power cables, Furukawa Review, 35 (2009) 18.
[30] Lightning Laboratory Information, NTS, http://www.nts.com/services/lightning, 2013 (2013).
[31] www, ABB Generator Circuit Breakers, http://www.abb.co.uk/product/us/9AAC30200091.aspx?country=GB, (2013).
[32] L. Brown, Cost-effective manufacturing: Joining of Cu and Cu-alloys, http://www.copperinfo.co.uk/design-and-manufacture/downloads/pub-98-joining-of-cu-and-cu-alloys.pdf, (1994).
[33] www, Alstom Electrical Arc Furnace Power Transformers, http://www.alstom.com/Global/Grid/Resources/Power%20Transformers/Documents/Electrical%20arc%20furnace%20Brochure%20GB.pdf, 2013 (2013).
[34] A.J. Dietz, W.E. Audette, L. Bromberg, J.V. Minervini, B.K. Fitzpatrick, Resistance of Demountable Mechanical Lap Joints for a HIgh Temperature Superconducting Cable Connector, IEEE Trans Appl Super, 18 (2008) 1171.
[35] Y. Zhang, R.C. Duckworth, T.T. Ha, M.J. Gouge, Solderability study of RABiTS-based YBCO coated conductors, Physica C, 471 (2011) 437.

[36] R. Tediosi, M. Alessandrini, C. Beneduce, S. Schneider, D. Eckert, Low Temperature and Magnetic Field Performance of Spliced Commercial YBCO CC, IEEE Trans. Appl. Supercond., 22 (2012) 6600804.
[37] C.M. Rey, R.C. Duckworth, Y. Zhang, Splice resistance measurements on 2G YBCO coated conductors, IEEE Trans. Appl. Supercond., 19 (2009) 2317.
[38] K. Natsume, Y. Terazaki, T. Mito, N. Yanagi, Y. Ogawa, J. Morikawa, K. Uchijima, Y. Hosaka, S. Nose, A. Tomioka, I. Itoh, E. Takada, M. Konno, M. Ohaku, Experimental Results of the HTS Floating Coil Using REBCO Tapes for the Mini-RT Upgrading, IEEE Trans. Appl. Supercond., 24 (2014) 4601104.
[39] Y. Seino, S. Ito, H. Oguro, H. Hashizume, Investigation of Influences of Film Resistance and Magnetic Field on Contact Resistance in a Mechanical Lap Joint of GdBCO Tapes, IEEE Trans. Appl. Supercond., 25 (2015) 6603405.
[40] SuperPower-Furukawa, SuperPower 2G HTS Coated Conductors, www.superpower-inc.com/content/2g-hts-wire, (2013).
[41] L. Bromberg, M. Tekula, L.A. El-Guebaly, R. Miller, ARIES Team, Options for the use of high temperature superconductor in tokamak fusion reactor designs Fusion Engineering and Design, 54 (2001) 167-180.
[42] SuperPower-Furukawa, Soldering HTS 2G tapes, http://www.superpower-inc.com/system/files/SP_Soldering+Instructions_2013FEC_v2.pdf, (2013).
[43] M. Hansen, K. Anderko, Constitutuion of Binary Alloys, McGraw-Hill Book Company, New York, 1958.
[44] T. Laurila, V. Vuorinen, J.K. Kivilahti, Interfacial reactions between lead-free solders and common base materials, Materials Science and Engineering, R49 (2005) 1.
[45] H.-S. Shin, A. Nisay, M.B. de Leon, M.J. Dedicatoria, Joining of REBCO coated conductor tapes using ultrasonic welding method, IEEE Trans. Appl. Supercond., 25 (2015).
[46] H.S. Shin, J.M. Kim, M.J. Dedicatoria, Pursuing low joint resistivity in Cu-stabilized $REBa_2Cu_3O_\delta$ coated conductor tapes by the ultrasonic weld-solder hybrid method, Supercond Sci Tech, 29 (2016) 015005.
[47] F.P. Incropera, D.P. De Witt, Fundamentals of heat and mass transfer, John Wiley and Sons, 1990.
[48] J.R. Davis, Alloying: Understanding the Basics, ASM International, 2001.
[49] H. Dreuth, H. Dederichs, Evaluation of low resistance contacts on $YBa_2Cu_3O_7$ thin films using the transmission line model, Superconductivity Science and Technology, 6 (1993) 464.
[50] M. Polak, P.N. Barnes, G.A. Levin, YBCO/Ag boundary resistivity in YBCO tapes with metallic substrates, Supercond Sci Tech, 19 (2006) 817-820.
[51] R. Jaramillo, T.F. Rosenbaum, E.D. Isaacs, O.G. Shpyrko, P.G. Evans, G. Aep[pli, Z. Cai, Microscopic and macroscopic signatures of antiferromagnetic domain walls, Phys. Rev. Lett., 98 (2007) 117206.
[52] J.W. Ekin, T.M. Larson, N.F. Bergren, A.J. Nelson, A.B. Swartziander, L.L. Kazmerski, A.J. Panson, B.A. Blankenship, High Tc superconductor/noble-metal contacts with surface resistivities in the 10^{-10} Ohm-cm^2 range, Applied Physics Letters, 52 (1988) 1819.
[53] G. Humpston, D.M. Jacobson, Indium solders, Advanced Materials & Processes, 163 (2005) 45.
[54] A. Mogro-Campero, K.W. Paik, L.G. Turner, Degradation of thin films of $YBa_2Cu_3O_7$ by annealing in air and in vacuum, Journal of Superconductivity, 8 (1995) 95.
[55] M.K. Kelly, S.-W. Chan, K. Jenkin, D.E. Aspnes, P. Barboux, J.-M. Tarascon, Optical characterization of surface and interface oxygen content in $YBa_2Cu_3O_x$, Applied Physics Letters, 53 (1988) 2333.
[56] B. Wuyts, V.V. Moshchalkov, Y. Bruynseraede, Resistivity and Hall effect of metallic oxygen-deficient $YBa_2Cu_3O_x$ films in the normal state, Physical Review B, 53 (1996).
[57] A.C. Mota, P. Visani, A. Pollini, Magnetic Properties of Proximity-Induced Superconducting Copper and Silver, Journal of Low Temperature Physics, 76 (1989).

[58] S.A. Keys, D.P. Hampshire, Characterisation of the transport critical current density for conductor applications, in: D. Cardwell, D. Ginley (Eds.) Handbook of Superconducting Materials, IOP Publishing, Bristol, 2003, pp. 1297-1322.
[59] D.M.J. Taylor, D.P. Hampshire, Relationship between the *n*-value and critical current in Nb_3Sn superconducting wires exhibiting intrinsic and extrinsic behaviour, Superconductor Science and Technology, 18 (2005) S297-S302.
[60] Z. Mei, H. Holder, H.A. Vander Plas, Low-Temperature Solders, Hewlett-Packard Journal, (1996) 10.
[61] R.C. Weast, M.J. Astle, W.H. Beyet, Handbook of Chemistry and Physics, 69th Edition ed., CRC Press, Boca Raton, FL, 1989.
[62] J.W. Ekin, Experimental Techniques for Low-Temperature Measurements, in, Oxford University Press, New York, 2007, pp. 58.
[63] Materials Properties, in: http://cryogenics.nist.gov/MPropsMAY/materialproperties.htm, 2013.
[64] J. Lu, E.S. Choi, H.D. Zhou, Physical properties of Hastelloy C-276 at cryogenic temperatures, Journal of Applied Physics, 103 (2008).
[65] R.R. Romanofsky, F.A. Miranda, Low Temperature Electronics: Physics, Devices, Circuits, and Applications, Academic Press, 2000.
[66] www.MatWeb.com, Thermal Conductivity of $In_{52}Sn_{48}$ solder, http://www.matweb.com/search/DataSheet.aspx?MatGUID=4c97435ecca248e2bd9e405fdb32b160&ckck=1, (2014).
[67] G.A. Shams, J.W. Cochrane, G.J. Russell, Thermal conductivity and thermoelectric power of high-quality $YBa_2Cu_3O_{7-delta}$ crystals, Physica C: Superconductivity, 363 (2001) 243.
[68] C.Y. Ho, R.W. Powell, P.E. Liley, Thermal conductivity of the elements, Journal of Physical and Chemistry Reference Data, 1 (1972) 279.
[69] N.S. Rudenko, L.W. Schubnikow, Viscosity of liquid nitrogen, carbon monoxide, argon and oxygen as a function of temperature, in, NASA, 1968.
[70] Brookhaven-National-Laboratory, Selected Cryogenic Data Notebook Section 6 BNL 10200-R, Vol. I, http://www.bnl.gov/magnets/staff/gupta/cryogenic-data-handbook/.
[71] R.W. Powers, M. R.W., H.L. Johnston, Thermal Conductivities of Condensed Gases. I. The Thermal Conductivity of Liquid Nitrogen between 65 and 90 °K, Journal of the American Chemical Society 76 (1954) 5968.
[72] A. Faghri, Y. Zhang, Transport Phenomena in Multiphase Systems, Academic Press Inc, 2006.
[73] R.J. Donnelly, C.F. Barenghi, The Observed Properties of Liquid Helium at the Saturated Vapor Pressure, Journal of Physical Chemistry Reference Data, 27 (1998) 1217.
[74] M.F. Merriam, Superconductivity in the Indium-Tin System, Physical Review, 131 (1963) 7.
[75] N.R. Werthamer, E. Helfand, P.C. Hohenberg, Temperature and Purity Dependence of the Superconducting Critical Field, H_{C2}. III. Electron Spin and Spin-Orbit Effects., Physical Review, 147 (1966) 295-302.